Clinical Cancer Research

Molecular Targeted Therapies Elicit Concurrent Apoptotic and GSDME-Dependent Pyroptotic Tumor Cell Death

Haijiao Lu[1,2], Shengzhe Zhang[3], Jie Wu[4], Minjiang Chen[5], Mei-Chun Cai[1], Yujie Fu[6], Wenfeng Li[7], Jing Wang[7], Xiaojing Zhao[6], Zhuang Yu[7], Pengfei Ma[1], and Guanglei Zhuang[1,2]

Abstract

Purpose: The induced death signals following oncogene inhibition underlie clinical efficacy of molecular targeted therapies against human cancer, and defects of intact cell apoptosis machinery often lead to therapeutic failure. Despite potential importance, other forms of regulated cell death triggered by pharmacologic intervention have not been systematically characterized.

Experimental Design: Pyroptotic cell death was assessed by immunoblot analysis, phase-contrast imaging, scanning electron microscopy, and flow cytometry. Tumor tissues of patients with lung cancer were analyzed using IHC. Functional impact of pyroptosis on drug response was investigated in cell lines and xenograft models.

Results: We showed that diverse small-molecule inhibitors specifically targeting KRAS-, EGFR-, or ALK-driven lung cancer uniformly elicited robust pyroptotic cell death, in addition to simultaneously invoking cellular apoptosis. Upon drug treatment, the mitochondrial intrinsic apoptotic pathway was engaged and the mobilized caspase-3 protease cleaved and activated gasdermin E (GSDME, encoded by *DFNA5*), which permeabilized cytoplasmic membrane and executed cell-lytic pyroptosis. GSDME displayed ubiquitous expression in various lung cancer cell lines and clinical specimens, including *KRAS*-mutant, *EGFR*-altered, and *ALK*-rearranged adenocarcinomas. As a result, cooccurrence and interplay of apoptosis and pyroptosis were widespread in lung cancer cells, succumbing to genotype-matched regimens. We further demonstrated that pyroptotic cell death partially contributed to the drug response in a subset of cancer models.

Conclusions: These results pinpoint GSDME-dependent pyroptosis as a previously unrecognized mechanism of action for molecular targeted agents to eradicate oncogene-addicted neoplastic cells, which may have important implications for the clinical development and optimal application of anticancer therapeutics. *Clin Cancer Res; 24(23); 6066–77. ©2018 AACR.*

Introduction

An emerging is that the intricate molecular regulation on the inherent signal-mediated death process, generally referred to as regulated cell death (1), dictates the malignant transformation and also therapeutic responses of human cancers (2, 3). For decades, apoptosis has been extensively studied as the predominant form of regulated cell death underlying tumor pathogenesis and therapies (4). During neoplasm development, cancer cells activate numerous oncogenic effectors to derive survival advantages by marshaling the pro-proliferative apparatus and countering the tendency for apoptosis (2, 5). On the contrary, cytotoxic anticancer drugs, especially molecular targeted agents that take advantage of the "oncogene addiction" phenomenon, may rewire particular signaling circuits to favor a caspases-directed apoptotic outcome, yielding tumor cell elimination (3, 6–10). As a result, pharmacologically blocking prosurvival components is considered an effective approach to improve therapeutic index of target-based monotherapy (11–13), whereas cancer-associated defects in apoptosis induction and execution contribute to a significant proportion of treatment failures (14–16).

The long-standing view of cell apoptosis as the standard regulated death-programming mechanism has changed, owing to recent discoveries of defined molecular pathways mediating necrotic types of cell death (17–19). For instance, necroptosis is activated by specific protein kinases, most crucially receptor-interacting protein kinase-1 (RIPK1) and downstream protein kinase receptor-interacting protein 3 (RIP3), which phosphorylates mixed lineage kinase domain-like protein (MLKL) to allow for its oligomerization and subsequently necroptotic disruption of plasma membrane (20–31). Pyroptosis, on the other hand, is

[1]State Key Laboratory of Oncogenes and Related Genes, Shanghai Cancer Institute, Ren Ji Hospital, School of Medicine, Shanghai Jiao Tong University, Shanghai, China. [2]Shanghai Key Laboratory of Gynecologic Oncology, Ren Ji Hospital, School of Medicine, Shanghai Jiao Tong University, Shanghai, China. [3]School of Biomedical Engineering & Med-X Research Institute, Shanghai Jiao Tong University, Shanghai, China. [4]Department of Pathology, The Affiliated Hospital of Qingdao University, Shandong, China. [5]Department of Respiratory Medicine, Peking Union Medical College Hospital, Peking Union Medical College, Chinese Academy of Medical Sciences, Beijing, China. [6]Department of Thoracic Surgery, Ren Ji Hospital, School of Medicine, Shanghai Jiao Tong University, Shanghai, China. [7]Department of Oncology, The Affiliated Hospital of Qingdao University, Shandong, China.

Note: Supplementary data for this article are available at Clinical Cancer Research Online (http://clincancerres.aacrjournals.org/).

H. Lu, S. Zhang, and J. Wu contributed equally to this article.

Corresponding Authors: Guanglei Zhuang, School of Medicine, Shanghai Jiao Tong University, Shanghai 200240, China. Phone: 213-420-8660; Email: zhuangguanglei@163.com; and Pengfei Ma, pengfei0820@163.com; and Zhuang Yu, Department of Oncology, The Affiliated Hospital of Qingdao University, Shandong 266000, China. E-mail: yuzhuang2002@163.com

doi: 10.1158/1078-0432.CCR-18-1478

Translational Relevance

Molecular targeted therapies act most effectively through stimulating tumor cell death, and it has been established that defects of intact apoptosis machinery often lead to therapeutic failure. Despite potential importance, other forms of regulated cell death triggered by pharmacologic intervention remain elusive. This work pinpoints GSDME-dependent cell pyroptosis as another widespread death mode underlying the anticancer efficacy of diverse molecular targeted agents. Drug-induced apoptotic and pyroptotic processes are concurrently activated through the mitochondria–caspases pathway and coopt with each other to execute tumor killing, providing a mechanistic rationale for future clinical development and optimal application of antineoplastic therapeutics.

ascribed to the proteolytic fragmentation of gasdermin D (GSDMD) by caspase-1/4/5/11 (32–34) and is lately demonstrated to also operate through caspase-3 cleavage of gasdermin E (GSDME; refs. 35, 36). Furthermore, other examples of regulated cell death, such as ferroptosis, parthanatos, oxytosis, cyclophilin D–dependent necrosis, autophagy, and ETosis, are each controlled by discrete signaling cascades (18). Therefore, from a therapeutic standpoint, additional opportunities may exist for exploiting nonapoptotic machinery to enhance sensitivity and overcome resistance toward molecular targeted therapies in cancer. However, it remains to be elucidated whether any variants of cellular demise are indeed associated with certain treatments, how they interact with apoptosis, and whether these alternative death modes are clinically relevant. In this study, we set out to tackle these questions by systematically characterizing various forms of regulated cell death in *KRAS*-, *EGFR*-, or *ALK*-driven lung cancers treated with alteration-matched small-molecule inhibitors.

Materials and Methods

Cell culture and reagents

Cell lines were obtained from the ATCC or Japanese Collection of Research Bioresources Cell Bank in 2015, where cell characterization (polymorphic short tandem repeat profiling) and contamination tests were performed. For the study, cells were used at passage 4 to 10, without further testing in lab. Cells were cultured in RPMI1640 (Invitrogen) supplemented with 1% GlutaMAX and 10% FBS (Gibco). Small-molecule inhibitors, including trametinib, erlotinib, ceritinib, dabrafenib, lapatinib, crizotinib, pictilisib, niraparib, zVAD-FMK, zDEVD-FMK, Q-VD-OPh, ferrostatin-1, chloroquine, cyclosporin A, necrostatin-1, ALLN, and a library of 180 compounds (37), were purchased from Selleck Chemicals. All inhibitors were reconstituted in DMSO (Sigma-Aldrich) at a stock concentration of 10 mmol/L, except chloroquine which was reconstituted in H_2O, and used to treat tumor cells at a final concentration of 5 μmol/L unless indicated otherwise. Lactate dehydrogenase (LDH) assays were performed using CytoTox 96 Non-Radioactive Cytotoxicity Assay Kit (Promega).

Patient samples

The study was conducted in accordance with ethical guidelines of U.S. Common Rule, and was approved by the Ethics Committee of Ren Ji Hospital (Shanghai, China) and The Affiliated Hospital of Qingdao University (Shandong, China). Written informed consent was acquired from all patients in this study. Fresh-frozen tumor samples were collected in surgery, and formalin-fixed and paraffin-embedded (FFPE) sections were obtained during pathologic examination. LDH concentrations were measured by clinical laboratory of The Affiliated Hospital of Qingdao University. CT images were provided by medical imaging department. Details of patient information were in Supplementary Tables S1–S4.

Plasmids and sgRNA

All plasmids were constructed using the Gibson Assembly Cloning Kit (New England Biolabs) and Gateway Cloning System (Invitrogen). GSDME mutations were generated using the Q5 Site-Directed Mutagenesis Kit (New England Biolabs) and verified by Sanger sequencing. CRISPR-Cas9 technology was employed to knock out indicated genes. Sequences of sgRNAs were provided in Supplementary Table S5. For gene overexpression or knockout experiments, HEK293T cells were cotransfected with 5 μg of lentiviral constructs, 5 μg of plasmid Δ8.9, and 3 μg of plasmid VSVG. Cells were incubated at 37°C and the medium was replaced after 12 hours. Virus-containing supernatant was collected 48 hours after transfection and supplemented with 8 μg/mL polybrene to infect target cells in 6-well dishes. Infected cells were selected with 2 to 5 μg/mL puromycin.

Western blot analysis

Cells or tissue samples were lysed in RIPA buffer (Tris pH 7.4 50 mmol/L, NaCl 150 mmol/L, NP-40 1%, SDS 0.1%, EDTA 2 μmol/L) containing proteinase inhibitors (Roche) and phosphatase inhibitors (Roche). For cellular fractionation, A549, PC9, and NCI-H3122 cells were fractionated with the Qproteome Cell Compartment Kit (Qiagen). The lysates (20-μg protein) were subjected to SDS-PAGE and Western blot analysis. Antibodies against the following proteins were used: caspase-3 (#9665), cleaved caspase-3 (#9579), PARP (#9532), vimentin (#5741), pMLKL-S358 (#91689), LC3A/B (#12741), GAPDH (#8884), and H3 (#12648;Cell Signaling Technology). GSDME antibodies were kindly provided by Shao Lab (National Institute of Biological Sciences, Beijing), or purchased from Abcam (ab215191).

IHC

IHC was performed on 5-μm-thick, FFPE tissue sections collected at The Affiliated Hospital of Qingdao University and Peking Union Medical College Hospital (Beijing, China), or lung cancer tissue microarrays (US Biomax). Slides were baked, deparaffinized in xylene, passed through graded alcohols, and antigen retrieved with 10 mmol/L citrate buffer, pH 6.0 in a steam pressure cooker. Preprocessed tissues were treated with peroxidase block (Dako) to quench endogenous peroxidase activity, blocked using protein block (Dako), and incubated with GSDME antibodies (Abcam). Slides were then washed in 50 mmol/L Tris-Cl, pH 7.4 and incubated with horseradish peroxidase–conjugated secondary antibody. Immunoperoxidase staining was developed using the DAB system according to the manufacturer's instructions (Dako). Slides were counterstained with hematoxylin, dehydrated in graded alcohol and xylene, and coverslipped using mounting solution.

Immunofluorescence microscopy

Tumor cells were fixed for approximately 15 to 20 minutes in 4% paraformaldehyde and permeabilized with 0.1% Triton X-100 (in PBS) for 10 minutes. After three PBS washes, cells were blocked with 2% BSA for 30 minutes at room temperature. Cells were then incubated with anti-GSDME antibody (Abcam) diluted in 2% BSA at 4°C overnight. After three PBS washes, the cells were incubated with 1 μg/mL Alexa Fluor 488–conjugated secondary antibodies and Alexa Fluor 594 Phalloidin (Invitrogen) in the dark for 1 hour. Cells were washed three times with PBS in the dark, stained with DAPI (Invitrogen) and mounted in Prolong Gold Antifade Reagent (Invitrogen). The immunofluorescent staining was observed using a confocal microscope (Leica).

Cell viability and apoptosis assays

Cell viability was analyzed using a Cell Titer-Glo Luminescent Cell Viability Assay Kit (Promega). For visualization, cells were fixed with formalin and stained with crystal violet. Cell apoptosis was detected using the Caspase-Glo 3/7 Assay Kit (Promega), Click-iT Plus TUNEL Assay Kit (Invitrogen), or the Dead Cell Apoptosis Kit staining Annexin V-FITC and propidium iodide (PI) followed by flow cytometry (Invitrogen). Flow cytometric analysis was performed on a FACSAria II cytometer (BD Biosciences) and data processed by FlowJo software.

Scanning electron microscopy

Cells grown on glass coverslips were washed with PBS buffer and fixed with 3% glutaraldehyde at 4°C overnight. Samples were dehydrated through a graded series of ethanol (50%, 70%, 80%, 95%, and 100%) and dried by Critical Point Dryer CPD 300 (Leica). Dried specimens were sputter coated with gold-palladium by Super Cool Sputter Coater SCD050 (Leica) and imaged with a scanning electron microscope S3400N-II (Hitachi) operating at 10 kV.

Tumor xenograft models

Indicated tumor cells (1×10^6) were mixed with Matrigel (BD Biosciences) and subcutaneously implanted in the dorsal flank of BALB/c nude mice. When tumor sizes reached approximately 200 mm^3, animals were randomized into two groups of 10 mice each. One group of mice was treated with vehicle control (0.5% methylcellulose and 0.2% Tween-80), and the other group was treated with ceritinib (NCI-H3122, 10 mg/kg/day) or erlotinib (HCC827, 10 mg/kg/day). Tumor volumes (10 animals/group) were measured with a caliper and calculated as length $\times$ width^2 $\times$ 0.52. The Institutional Animal Care and Use Committee of Ren Ji Hospital approved all animal protocols.

Statistical analysis

Statistical analysis was performed with GraphPad Prism software. In all experiments, comparisons between two groups were based on two-sided Student *t* test and one-way ANOVA was used to test for differences among more groups. *P* values of <0.05 were considered statistically significant.

Results

Diverse molecular targeted therapies induce tumor cell pyroptosis

The notion that antitumor therapeutics act most potently through stimulating apoptosis prompted us to comprehensively investigate different subroutines of regulated cell death that likely occur in response to targeted agents. To this end, A549 (harboring $KRAS^{G12S}$), PC9 (harboring $EGFR^{E746\text{-}A750\ del}$), and NCI-H3122 (harboring *EML4-ALK* fusion gene) cells were selected to represent three common pathogenic scenarios for patients with lung cancer (38), where trametinib (a MEK inhibitor), erlotinib (an EGFR inhibitor), or ceritinib (an ALK inhibitor) served as genotype-matched treatments, respectively. As expected, all cell lines responded well to these tailored drugs targeting specific oncogenic aberrations (Supplementary Fig. S1A). We individually combined a range of small-molecule inhibitors to determine their agonistic or antagonistic roles, and found that cell death induced by targeted therapies was appreciably prevented by the pan-caspase inhibitor Q-VD-OPh (39), whereas necrostatin-1 (an inhibitor of necroptosis; ref.21), ferrostatin-1 (an inhibitor of ferroptosis; ref. 40), niraparib (an inhibitor of parthanatos; ref 41), ALLN (an inhibitor of oxytosis; ref. 42), cyclosporine A (an inhibitor of cyclophilin D–dependent necrosis; ref. 43), and chloroquine (an inhibitor of autophagy; ref. 44) did not exhibit consistent effects (Supplementary Fig. S1A). In agreement with these results, concomitant cleavage of caspase-3 and PARP (a marker of cells undergoing apoptosis), but no changes of MLKL phosphorylation (a marker for cell necroptosis) or LC3 lipidation (a marker for cell autophagy), was observed in A549, PC9, and NCI-H3122 cells upon compound exposure (Fig. 1A). Interestingly, reminiscent of characteristic pyroptotic cell morphology, we noted evident balloon-like bubbles that were distinct from classic apoptotic blebbing (Fig. 1B). A closer inspection of drug-damaged cells using high-resolution scanning electron microscopy revealed vigorous membranous protrusions (Fig. 1C), described previously as pyroptotic bodies (45). Recent studies have established that pyroptosis can be executed by proteolytically processed GSDME upon activation of caspase-3 during apoptosis (35, 36), and indeed, GSDME was cleaved to generate N-terminal fragments following pharmacologic inhibition, with comparable kinetics with that of caspase-3 or PARP cleavage (Fig. 1A). Similar findings were obtained with erlotinib-treated HCC827 (harboring $EGFR^{E746\text{-}A750\ del}$), trametinib-treated NCI-H358 (harboring $KRAS^{G12C}$), trametinib-treated HCC44 (harboring $KRAS^{G12C}$), and crizotinib-treated NCI-H1648 (harboring *MET* gene amplification;Supplementary Fig. S1B). Moreover, the swelling cells displayed LDH release at a time-dependent manner, indicating plasma membrane rupture and leakage (Fig. 1D). Flow cytometric analysis verified the necrotic nature of treatment-induced cell death, as exemplified by Annexin V and PI double-positive staining (Fig. 1E). These data suggested that diverse molecular targeted therapies, besides triggering apoptosis, could also lead to tumor cell pyroptosis.

Ubiquitous expression and functional implications of GSDME in lung cancer

GSDME, causally implicated in an autosomal-dominant heritable deafness (46), is a newly recognized executor of cell pyroptosis and reportedly silenced in several cancers as a putative tumor suppressor due to promoter hypermethylation (47–49). Nevertheless, the expression level and pattern of GSDME in different genetically defined lung cancer clusters is currently unexplored. In contrast to previous observations that no or little GSDME was expressed within other tumor types (47–49), GSDME protein was readily detected by immunoblot analysis in most lung cancer cell lines disregarding oncogenic drivers (Fig. 2A). We subjected this large panel of carcinoma models to their alteration-specific targeted inhibition, and uncovered that

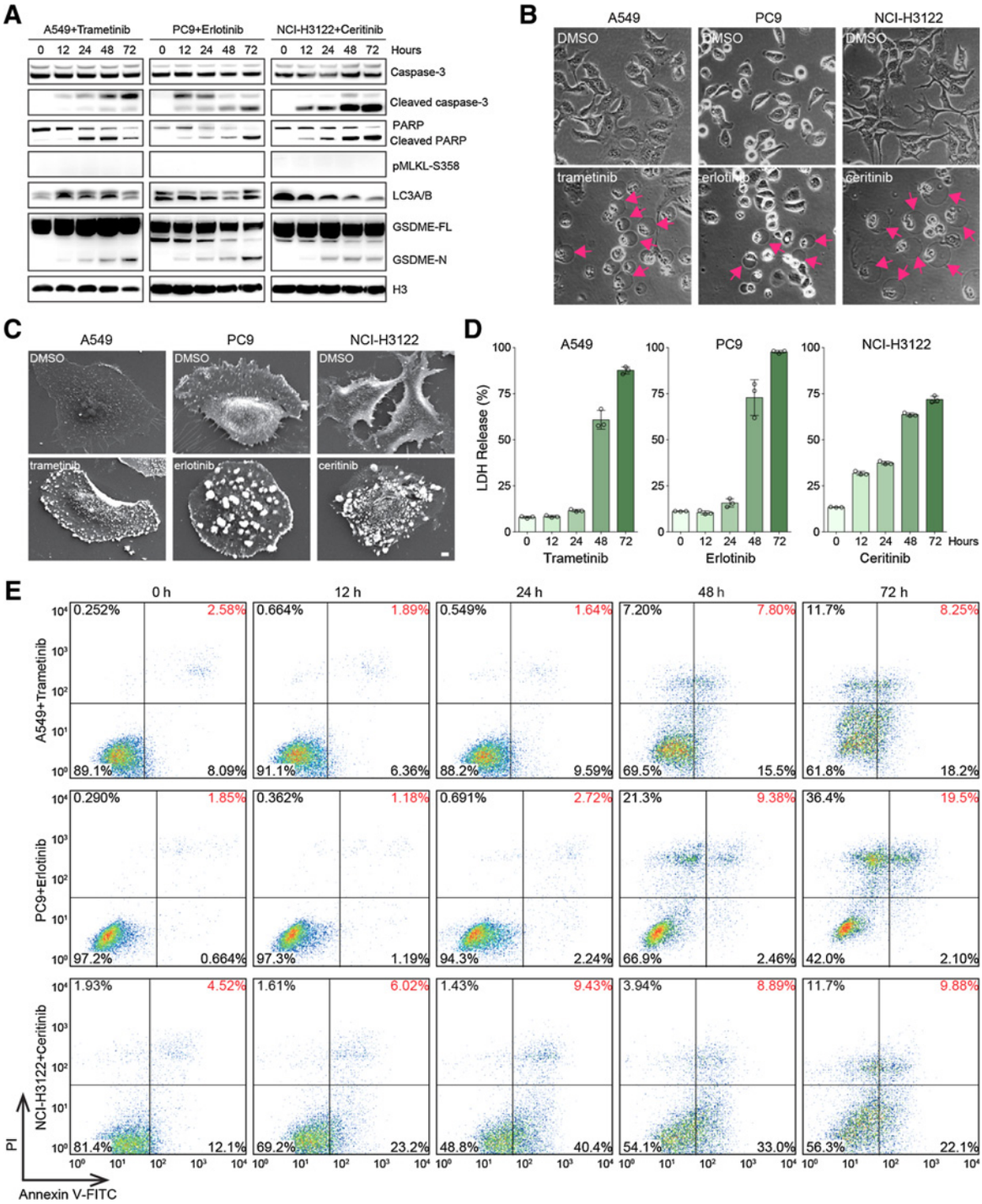

Figure 1.

Diverse molecular targeted therapies induce tumor cell pyroptosis. **A,** A549, PC9, and NCI-H3122 were treated with trametinib, erlotinib, and ceritinib, respectively. The indicated proteins were analyzed by immunoblotting. Time-dependent cleavage of caspase-3, PARP, and GSDME was demonstrated. GSDME-FL, full-length GSDME; GSDME-N, GSDME N-terminal domain. **B,** Phase-contrast imaging of A549, PC9, and NCI-H3122 cells treated with DMSO or indicated inhibitors. Pyroptotic cell morphology was pinpointed by red arrows. **C,** Representative scanning electronic microscopy images of A549, PC9, and NCI-H3122 cells treated with DMSO or indicated inhibitors. Note membranous protrusions, described previously as pyroptotic bodies, in drug-treated cells. **D,** LDH release from A549, PC9, and NCI-H3122 cells treated with indicated inhibitors. Each column represented the mean value of three biological replicates, and error bars indicated SD. **E,** Flow cytometry analysis of inhibitor-treated A549, PC9, and NCI-H3122 cells stained by Annexin V-FITC and PI. The percentage of double-positive cells, presumably pyroptotic cells, was labeled in red.

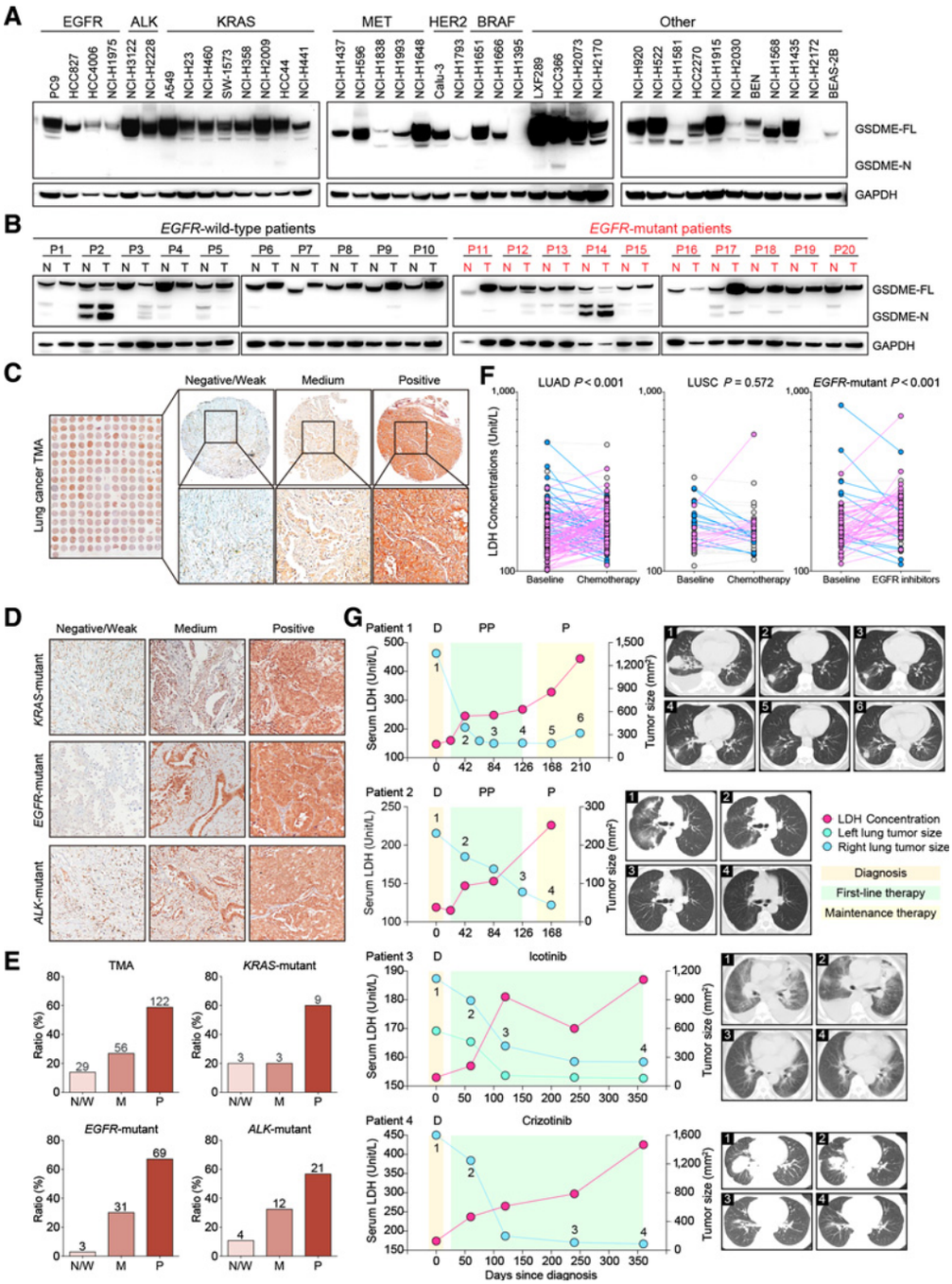

Figure 2.

Ubiquitous expression and functional implications of GSDME in lung cancer. **A,** GSDME expression was analyzed by immunoblotting in a panel of lung cancer cell lines with indicated oncogenic alterations on the top. **B,** GSDME expression was analyzed by immunoblotting in paired normal lung (N) and tumor tissues (T) collected from 10 *EGFR*-mutation-positive and 10 *EGFR* mutation–negative patients. **C,** IHC staining of GSDME in a lung cancer TMA that contained 208 specimens. Representative images for negative/weak, medium, or positive IHC staining were shown. **D,** IHC staining of GSDME in a cohort of 155 patients affected by *KRAS*-mutant, *EGFR*-altered, or *ALK*-rearranged lung cancer. Representative images for negative/weak, medium, or positive IHC staining are shown. N/W, negative/weak staining; M, medium staining; P, positive staining. **E,** Quantification of GSDME expression status on the basis of IHC staining. **F,** Serum LDH concentrations of patients with lung cancer at diagnosis and postchemotherapy or EGFR inhibitors. Pink lines indicated LDH-elevated cases [(LDHpost-LDHpre)/LDHpre>10%]; blue lines indicated LDH-reduced cases [(LDHpost-LDHpre)/LDHpre←10%]; gray lines indicated LDH-unchanged cases [-10%< (LDHpost-LDHpre)/LDHpre<10%]. A significant increase of serum LDH was associated with therapeutic treatment in adenocarcinomas or EGFR-mutant lung cancer, but not squamous cell carcinomas. Statistical significance was determined by paired Student *t* test. **G,** Examples of patients showing accompanied LDH release and cancer regression during genotype-matched clinical treatments. Tumor sizes were measured on CT images. PP, pemetrexed + cisplatin; P, pemetrexed.

LDH was almost universally, albeit to differential extents, released into the culture supernatants (Supplementary Fig. S2A). The efficiency of LDH release depended on not only drug efficacy but also GSDME expression (Supplementary Fig. S2B), suggesting that GSDME was truly operative to mediate therapy-induced pyroptotic cell death. To evaluate the clinical relevance of GSDME in patients with lung cancer, we conducted The Cancer Genome Atlas (TCGA) pan-cancer genomic interrogation and did not identify prevalent copy number abnormalities or somatic mutations across 20 major human malignancies (Supplementary Fig. S3A). By analyzing gene transcription data in TCGA lung adenocarcinomas, we found that *DFNA5* (encoding GSDME) was modestly upregulated in *EGFR*-mutant neoplasms, but downregulated in *STK11*- or *KEAP1*/*NFE2L2*-mutant tumors, as compared with the respective wild-type counterparts (Supplementary Fig. S3B). At the protein level, GSDME was ubiquitously expressed in paired normal lung and tumor tissues collected from 10 *EGFR* mutation–positive and 10 *EGFR* mutation–negative patients (Fig. 2B). Notably, multiple treatment-naïve samples presented spontaneous GSDME cleavage for yet-to-be understood reasons (Fig. 2B). Cellular fractionation assays showed that nearly all endogenous GSDME resided in the cytosolic compartment (Supplementary Fig. S3C), which was further confirmed by immunofluorescent staining (Supplementary Fig. S3D). Using this validated GSDME antibody, we performed IHC evaluation of a lung cancer tissue microarray (TMA) that contained 208 specimens belonging to varied histotypes with unknown genetic information (Fig. 2C; Supplementary Table S1). In addition, GSDME status was assessed in a cohort of 155 individuals affected by *KRAS*-mutant, *EGFR*-altered, or *ALK*-rearranged lung cancer (Fig. 2D; Supplementary Table S2). GSDME exhibited pervasive expression (Supplementary Fig. S4), as evidenced by positive IHC staining in 58.9% of TMA cases, 60.0% of *KRAS*-mutant cases, 67.0% of *EGFR*-mutant cases, and 56.8% of *ALK*-mutant cases (Fig. 2E). As with GSDME in cell lines, the protein was plausibly functional in patients with lung cancer, because serum LDH concentrations significantly increased during 6-month follow-up after initial chemo- or EGFR inhibitor-based treatment (Supplementary Tables S3 and S4), with the exception of squamous cell carcinomas that were known to typically resist chemotherapy (Fig. 2F). Although multiplex factors likely contributed to the elevated LDH levels, a fraction of subjects showed accompanying dramatic cancer regression (Fig. 2G), highlighting a circumstance where drug-related tumor cell death, at least partially, accounted for the LDH release. We concluded that the widespread GSDME expression among diverse molecular subtypes of lung cancer underscored the potential biological importance of tumor cell pyroptosis in disease course and clinical management.

Molecular targeted therapies activate the mitochondrial intrinsic apoptotic pathway to elicit GSDME-dependent pyroptosis

We sought to explicitly define the molecular mechanism by which cellular pyroptosis was instigated under the action of various inhibitors. Validating recent findings that GSDME was a critical substrate of caspase-3 and a key mediator of nonimmune cell pyroptosis (35, 36), *DFNA5* or *CASP3* depletion using the clustered regularly interspaced short palindromic repeats (CRISPR)-Cas9 system in A549, PC9, or NCI-H3122 (Fig. 3A) significantly reduced necrosis-associated LDH release (Fig. 3B) and characteristic ballooning of the cell membrane (Supplementary Fig. S5A). Similarly, combined treatment with targeted therapeutics and the pan-caspase inhibitor zVAD or caspase-3–specific inhibitor zDEVD considerably abrogated extracellular release of LDH (Supplementary Fig. S5B), proteolytic cleavage of GSDME, and balloon-like swelling of treated cells (Supplementary Fig. S5C). Conversely, ectopic *DFNA5* overexpression was sufficient to enhance GSDME cleavage in NCI-H2009, HCC4006, and HCC827 following drug administration (Fig. 3C), and as a consequence, lead to markedly increased LDH release (Fig. 3D) and more pronounced pyroptotic cell morphology (Supplementary Fig. S6A). In addition to caspase-3, we individually knocked out each of the pivot components within mitochondrial intrinsic apoptotic pathway and revealed that a myriad of genes disturbed treatment-induced LDH release in A549 cells (Supplementary Fig. S6B). A central signaling axis, that is, BIM–BAX–cytochrome c-APAF1–Smac–caspase-9–caspase-3–GSDME, was pinpointed to evidently regulate the pyroptotic process. Indeed, genetic deletion of these core members resulted in limited amount of released LDH (Fig. 3E) and notable deficits of GSDME fragmentation (Fig. 3F) in all the three tested cell models. Therefore, by activating the mitochondrial intrinsic apoptotic pathway, molecular targeted therapies facilitated caspase-3 cleavage of GSDME to elicit pyroptotic cell death.

Pyroptosis cooccurs and interacts with apoptosis

An important question emerged as to how tumor cell apoptosis and pyroptosis were coopted and orchestrated in the context of targeted agents, considering that the two processes shared the same regulatory machinery. Even though the terminal morphology of GSDME-expressing cells exclusively resembled that observed in typical pyroptotic death, presumably due to the loss of plasma membrane integrity, the initial reports that identified apoptosis-coupled pyroptosis reached somewhat divergent conclusions. On one hand, GSDME-mediated pyroptosis was considered the secondary necrosis provided that apoptotic cells were not scavenged (35). On the other hand, it was hypothesized that therapy-induced pyroptosis might precede or even impede apoptosis, such that only GSDME-deficient cells were redirected or released to produce an apoptotic outcome (36). Distinct from these previous conceptions, we argued it was plausible to speculate that the two forms of regulated cell death were contemporaneously mobilized by anticancer therapies. In agreement with this hypothesis, when drug-exposed adherent cells and supernatant cells were separately analyzed (Fig. 4A), the biochemical markers for apoptosis and pyroptosis were invariably synchronously detected. Specifically, adherent cells mainly underwent early apoptotic/pyroptotic events on the basis of limited caspase-3/PARP/GSDME fragmentation (Fig. 4B), whereas supernatant cells represented fully apoptotic/pyroptotic corpses as indicated by complete caspase-3/PARP/GSDME cleavage and homogeneous ballooning morphology (Fig. 4A). The concurrency was reassured by the quantification of terminal deoxynucleotidyl transferase dUTP nick end-labeling positive apoptotic cells (Supplementary Fig. S7A). To further corroborate this point, we screened a large panel of 180 small-molecule inhibitors to probe their deferential impact on trametinib-incited apoptosis and pyroptosis in A549 cells. Interestingly, the mitochondrial intrinsic apoptotoic pathway and its interconnected pyroptotic signal, both responsible for tumor cell eradication (Supplementary Fig. S7B), were always simultaneously activated, as evidenced by a

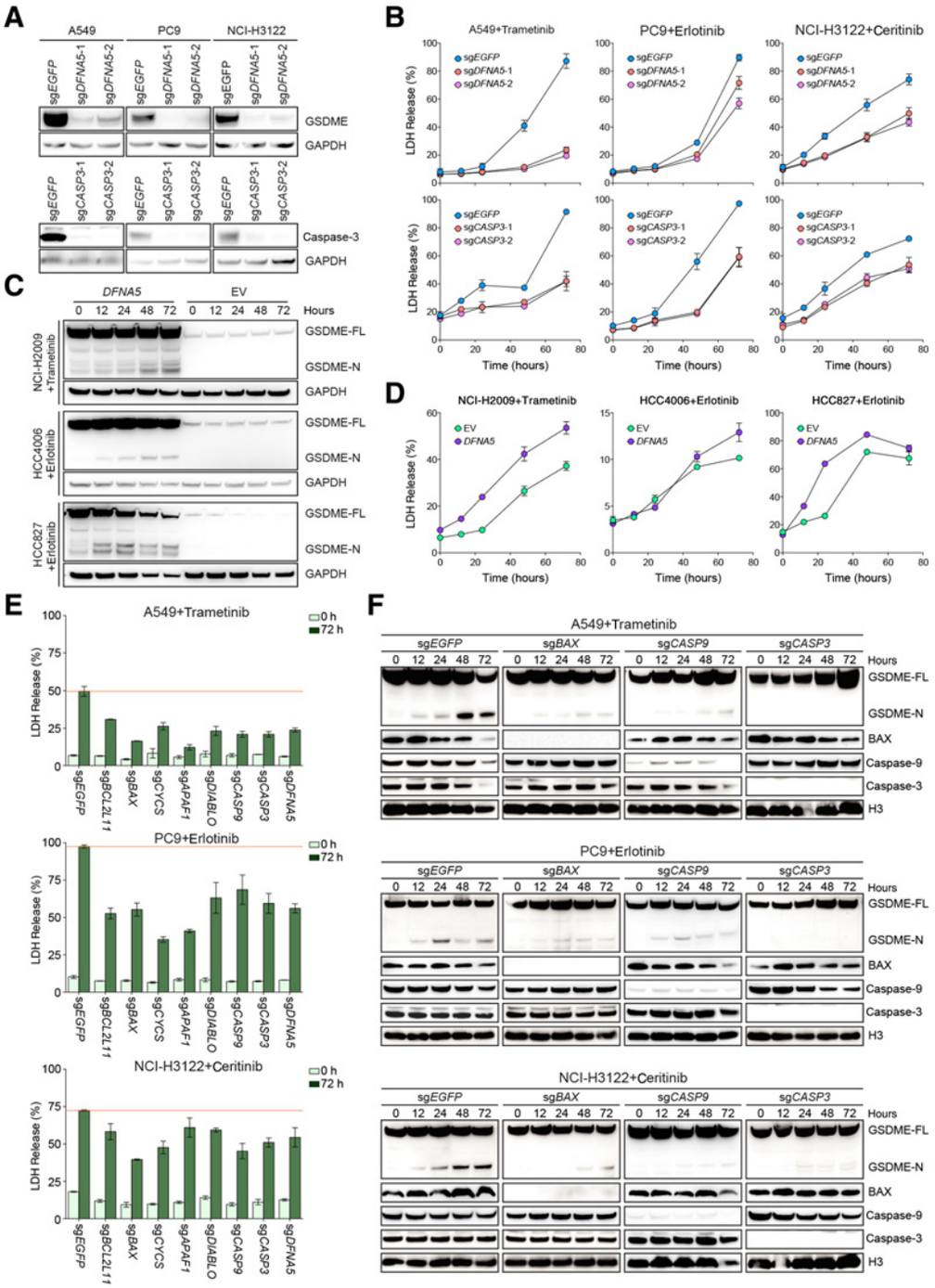

Figure 3.

Molecular targeted therapies activate the mitochondrial intrinsic apoptotic pathway to elicit GSDME-dependent pyroptosis. **A,** *DFNA5* or *CASP3* gene was knocked out in A549, PC9, and NCI-H3122 cells using CRISPR-Cas9 system, and GSDME or caspase-3 protein was analyzed by immunoblotting. **B,** *DFNA5* or *CASP3* gene was knocked out in A549, PC9, and NCI-H3122 cells using CRISPR-Cas9 system, and LDH release in the presence of indicated inhibitors was assayed. Each line represented the mean value of three biological replicates, and error bars indicated SD. **C,** *DFNA5* gene was overexpressed in NCI-H2009, HCC4006, and HCC827 cells. Cells were treated as indicated and GSDME protein was analyzed by immunoblotting. EV, empty vector. **D,** *DFNA5* gene was overexpressed in NCI-H2009, HCC4006, and HCC827 cells, and LDH release in the presence of indicated inhibitors was assayed. Each line represented the mean value of three biological replicates, and error bars indicated SD. **E,** LDH release in trametinib-treated A549, erlotinib-treated PC9, or ceritinib-treated NCI-H3122 cells with genetic depletion of indicated apoptotic genes. Each column represented the mean value of three biological replicates, and error bars indicated SD. **F,** *BAX, CASP9,* or *CASP3* gene was knocked out in A549, PC9, and NCI-H3122 cells, which were subsequently treated with trametinib, erlotinib, and ceritinib, respectively. The indicated proteins were analyzed by immunoblotting. Impaired cleavage of GSDME upon gene knockout was demonstrated.

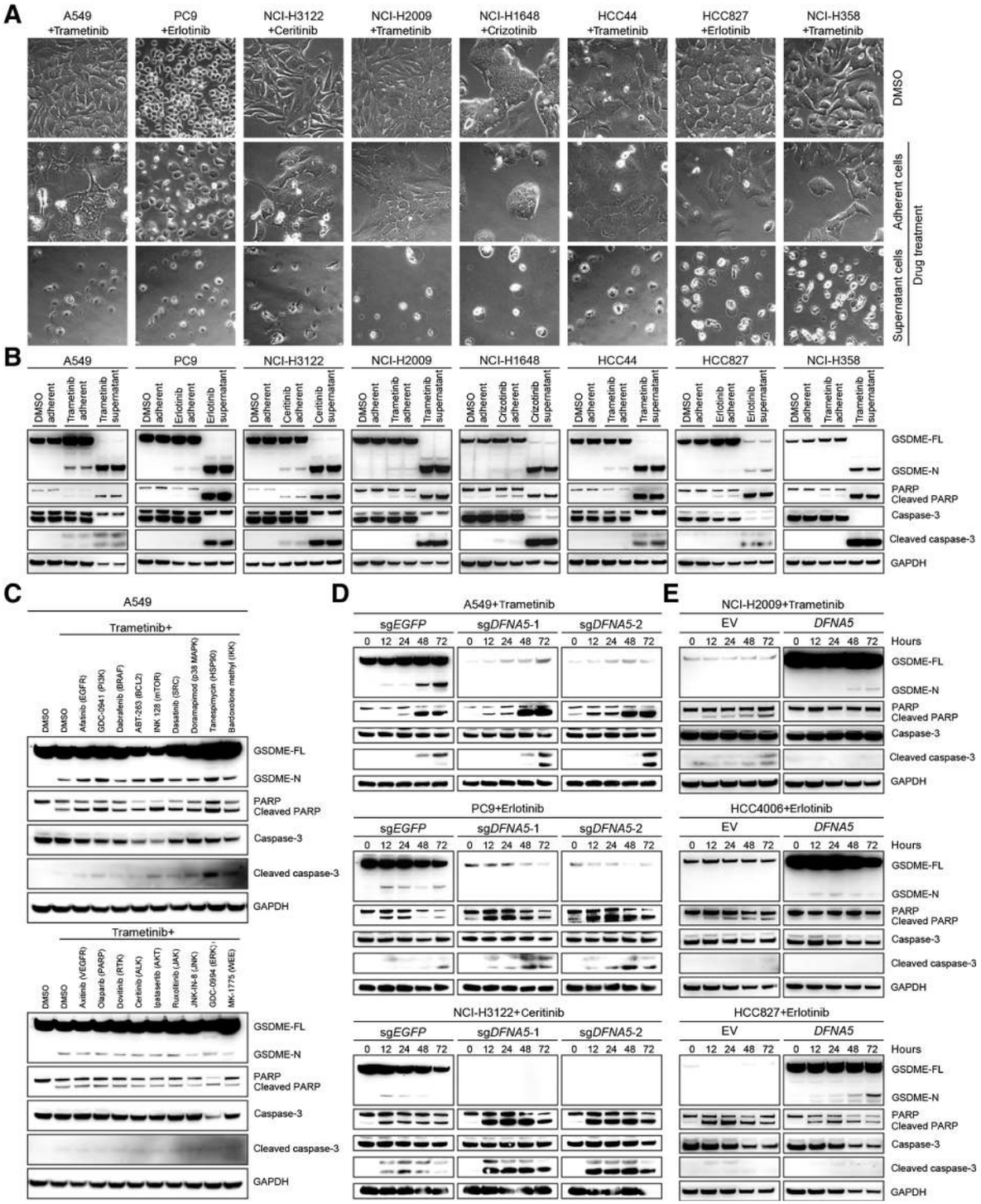

Figure 4.

Pyroptosis cooccurs and interacts with apoptosis. **A,** Lung cancer cell lines were treated with indicated inhibitors for 72 hours. Drug-treated adherent and supernatant cells were separately collected and imaged. **B,** Lung cancer cell lines were treated with indicated inhibitors for 72 hours, and drug-treated adherent and supernatant cells were separately collected. The protein markers for pyroptosis and apoptosis were analyzed by immunoblotting. Complete cleavage of caspase-3, PARP, and GSDME in drug-treated supernatant cells was noted. **C,** A549 cells were treated with trametinib either alone or in combination with indicated inhibitors (500 nmol/L). The indicated proteins were analyzed by immunoblotting. A concordant cleavage pattern of GSDME and PARP was demonstrated across drug combos. **D,** Western blot analysis of indicated proteins in inhibitor-treated A549, PC9, and NCI-H3122 cells with or without *DFNA5* deletion. **E,** Western blot analysis of indicated proteins in inhibitor-treated NCI-H2009, HCC4006, and HCC827 cells with or without *DFNA5* overexpression.

concordant cleavage pattern of caspase-3, PARP, and GSDME (Fig. 4C). We also reasoned that a conceivable interplay between cell pyroptosis and apoptosis might exist. Consistent with this possibility, we found that drug-treated *DFNA5* knockouts yielded more cleaved PARPs (Supplementary Fig. S7C) and caspase-3 products (Fig. 4D). In contrast, inhibitor-triggered PARP and caspase-3 cleavage was dampened in NCI-H2009, HCC4006, and HCC827 cells overexpressing *DFNA5* (Fig. 4E). Despite elusive mechanistic underpinnings, our data implied that pyroptosis was proficient in modulating apoptosis, reinforcing their string of cooccurrence in therapy-executed tumor cells. On the basis of these results, we proposed that targeted treatment likely dictated concomitant apoptosis and pyroptosis at the molecular level through the identical upstream pathway, and the existence of their potential signaling cross-talks could not be precluded.

Pyroptosis contributes to the antineoplastic efficacy of targeted agents

Given that GSDME expression and drug-induced pyroptosis were widespread in lung cancer, we tested whether GSDME-mediated pyroptotic cell death contributed to the anticancer effects of targeted therapies. As anticipated, genetic *DFNA5* deletion attenuated drug response and produced more drug-tolerant persisters (50) as assessed by crystal violet staining, most prominently in A549, NCI-H3122, and NCI-H358 cells (Fig. 5A), whereas *DFNA5* overexpression conversely tended to promote inhibitor sensitivity, for example, in A549, HCC827, and HCC44 cells (Fig. 5B). However, it was noteworthy that in the presence of intact apoptotic function, the prodeath effects of cell pyroptosis were overall modest and only observed in a subset of tumor models following driver inhibition. Nevertheless, the *in vitro* function of therapy-engaged pyroptosis was substantiated by *in vivo* results, which showed partially impaired treatment efficacy upon *DFNA5* knockout in NCI-H3122 cells (Fig. 5C) and an opposite improvement of therapeutic index following exogenous *DFNA5* expression in HCC827 cells (Fig. 5D). Of note, GSDME by itself did not impact on tumor growth in the absence of drug administration. The clinical significance of pyroptotic cell death in patients with cancer receiving targeted agents warranted prospective investigations.

Discussion

This study (summarized in Fig. 5E) has expanded the conventional view regarding apoptosis as the solely death route underlying molecular targeted therapeutics, established potential clinical relevance of GSDME expression and pyroptotic process in lung cancer, shed light on the interrelation between drug-induced pyroptosis and apoptosis, and proposed a functional role for pyroptosis in antitumor treatment.

We have provided several lines of evidence to support GSDME-dependent pyroptosis as a universal mechanism of action for molecular targeted agents to exterminate oncogene-addicted neoplastic cells. First, GSDME, the recently defined pyroptosis executor (35, 36), was ubiquitously expressed in the majority of lung cancer cell lines and primary tumor tissues, including *KRAS*-, *EGFR*-, or *ALK*-driven adenocarcinomas. Analysis of GSDME in the TCGA dataset revealed an upregulation in *EGFR*-mutant, and a downregulation in *STK11*- or *KEAP1*/*NFE2L2*-mutant patients. The mechanistic underpinning and possible association with therapeutic sensitivity remain to be elucidated. In contrast to our results, previous reports showed that GSDME expression was generally undetectable in various human cancers due to epigenetic gene silencing (47–49). Notably, several studies mainly used *in vitro* systems or invalidated antibodies, whereas we assayed a comprehensive cohort of lung carcinoma specimens utilizing a validated antibody on the basis of GSDME depletion by CRISPR-Cas9 technique, and therefore, different models and reagents could explain the discrepancy. Second, a wide range of genotype-guided treatments yielded GSDME cleavage and LDH-releasing pyroptosis, the efficiency of which was dependent on both drug efficacy and GSDME levels. Although lung cancer was exclusively investigated in light of recent progression on targeted medicine, we envision that a similar phenotype may be observed in other malignancies with tailored therapies. Thus, serum LDH and cleaved GSDME may potentially be explored as noninvasive pharmacodynamics or predictive biomarkers for chemotherapy and molecular regimens. Third, our data demonstrated that the mitochondrial intrinsic apoptotic pathway also mediated GSDME-dependent pyroptosis in the context of molecular inhibitors, and these two processes were executed at the same time. As a result, differential availability and activity of downstream effectors, rather than upstream triggers, most likely determine the temporal dynamics and terminal form of cell death following caspase-3 activation. Finally, cell pyroptosis induced by molecular targeted therapies, at least partially, contributed to their antineoplastic efficacy, a notion that was reasonable to speculate but needed formal approval. Importantly, we showed that chemotherapy or EGFR inhibitors increased serum LDH concentrations, accompanied by imaging-verified disease regression, implying that tumor cell pyroptosis might be functionally operative in patients with lung cancer during medical treatment. Although GSDME appeared to only marginally affect drug responsiveness, at least two factors could account for the relatively limited effects. Either apoptosis or pyroptosis alone was sufficient for driving cell death and interfering GSDME perhaps altered the apoptotic process. Alternatively, unknown mediators of pyroptosis other than GSDME or additional forms of necrotic death might make way to achieve cell killing in the absence of GSDME. We propose that molecular targeted therapies trigger different types of regulated cell death to cooperatively, rather than mutually exclusively, eliminate tumor cells.

Our findings may not only hold enormous promise for developing and optimizing cancer therapies, but also open up new avenues for future research. The preliminary observation of signaling interrelation between pyroptosis and apoptosis suggests that the two death modes may reciprocally regulate each other to produce cytotoxic inhibition. Thus, further understanding the molecular mechanism of this cross-talk has important implications for the rational application of targeted antitumor agents. In addition, how GSDME expression and function are physiologically modulated is yet to be defined, which would inform the appropriate means for manipulating the choice and intensity of tumor cell pyroptosis to maximize its translational capacity. Moreover, the updated paradigm for treatment-conferred cell death raises the possibility that a variety of therapeutic regimens may display the propensity

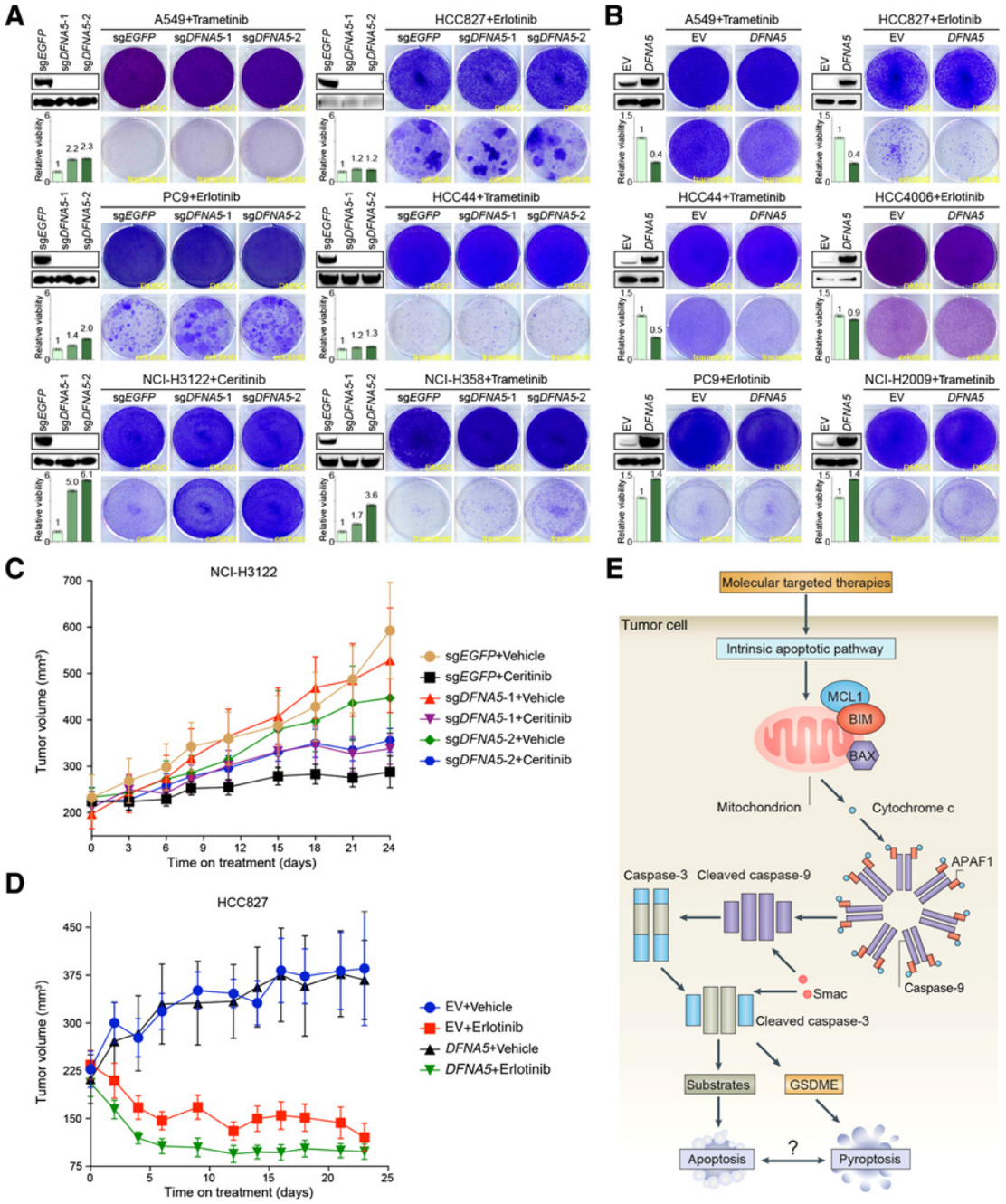

Figure 5.

Pyroptosis contributes to the antineoplastic efficacy of targeted agents. **A,** *DFNA5* gene was knocked out in indicated cell lines, and GSDME protein was analyzed by immunoblotting (upper band: GSDME; lower band: GAPDH). Drug response upon *DFNA5* depletion was assessed by crystal violet staining and quantified as shown in bar graphs with effect size labeled on the top. Relative viability was defined as the percentage of remaining cells upon drug treatment in each condition divided by the percentage of remaining cells in the sg*EGFP* group. **B,** *DFNA5* gene was overexpressed in indicated cell lines, and GSDME protein was analyzed by immunoblotting (upper band: GSDME; lower band: GAPDH). Drug response upon *DFNA5* overexpression was assessed by crystal violet staining and quantified as shown in bar graphs with effect size labeled on the top. Relative viability was defined as the percentage of remaining cells upon drug treatment in each condition divided by the percentage of remaining cells in the EV group. **C,** Tumor growth of *DFNA5*-depleted NCI-H3122 xenografts that were treated with ceritinib. Each line represented mean tumor volume of the respective group, and error bars indicated SD (10 mice/group). **D,** Tumor growth of HCC827 xenografts that ectopically expressed *DFNA5* gene and were treated with erlotinib. Each line represented mean tumor volume of the respective group, and error bars indicated SD (10 mice/group). **E,** A schematic summary of this study, showing that through activating the mitochondrial intrinsic apoptotic pathway, molecular targeted therapies could elicit concurrent apoptosis and GSDME-dependent pyroptosis. The potential molecular cross-talk between apoptosis and pyroptosis would require further characterization. The graph was adapted from Nature Reviews Immunology 2007; 7:532–42 by permission of Nature Publishing Group.

to invigorate immune responses by stimulating proinflammatory pyroptosis. The mold and equilibrium of regulated cell death and associated efferocytosis presumably determine the ultimate immunogenic properties of drug-treated tumors, a concept that can be exploited to assist strategizing the combined use of immunotherapy. Finally, as shown for chemotherapy (36), certain clinical toxicities may be likewise attributable to unintended normal cell pyroptosis caused by targeted cancer therapies. The identification and understanding of such side effects would provide the unprecedented opportunity to prevent, ameliorate, and manage them.

Disclosure of Potential Conflicts of Interest

No potential conflicts of interest were disclosed.

Authors' Contributions

Conception and design: H. Lu, W. Li, J. Wang, Z. Yu, P. Ma, G. Zhuang
Development of methodology: J. Wu
Acquisition of data (provided animals, acquired and managed patients, provided facilities, etc.): H. Lu, S. Zhang, J. Wu, Y. Fu, W. Li, J. Wang, X. Zhao, Z. Yu, P. Ma
Analysis and interpretation of data (e.g., statistical analysis, biostatistics, computational analysis): H. Lu, J. Wu, M.-C. Cai, W. Li, Z. Yu, P. Ma
Writing, review, and/or revision of the manuscript: H. Lu, M. Chen, P. Ma, G. Zhuang
Administrative, technical, or material support (i.e., reporting or organizing data, constructing databases): S. Zhang
Study supervision: G. Zhuang

Acknowledgments

This work was supported by the National Natural Science Foundation of China (81472537 and 81672714 to G. Zhuang; 81802734 to P. Ma; 81802809 to M.-C. Cai; 81702292 to M. Chen), Shanghai Municipal Education Commission-Gaofeng Clinical Medicine Grant Support (20161313 to G. Zhuang), Collaborative Innovation Center for Translational Medicine at Shanghai Jiao Tong University School of Medicine, the Shanghai Institutions of Higher Learning (Eastern Scholar to G. Zhuang), Shanghai Rising-Star Program (16QA1403600 and 81672714 to G. Zhuang), Shanghai Sailing Program (18YF1413200 and 81802734 to P. Ma), Shanghai Municipal Commission of Health and Family Planning (20174Y0043 and 81802809 to M.-C. Cai), and the State Key Laboratory of Oncogenes and Related Genes (SB17-06 to M.-C. Cai). We would like to thank Drs. Feng Shao, Yupeng Wang, and Trever G. Bivona for reagents, discussion, and critical reading of the manuscript.

The costs of publication of this article were defrayed in part by the payment of page charges. This article must therefore be hereby marked *advertisement* in accordance with 18 U.S.C. Section 1734 solely to indicate this fact.

Received May 11, 2018; revised July 6, 2018; accepted July 23, 2018; published first July 30, 2018.

References

1. Galluzzi L, Bravo-San Pedro JM, Vitale I, Aaronson SA, Abrams JM, Adam D, et al. Essential versus accessory aspects of cell death: recommendations of the NCCD 2015. Cell Death Differ 2015;22:58–73.
2. Hanahan D, Weinberg RA. Hallmarks of cancer: the next generation. Cell 2011;144:646–74.
3. Montero J, Sarosiek KA, DeAngelo JD, Maertens O, Ryan J, Ercan D, et al. Drug-induced death signaling strategy rapidly predicts cancer response to chemotherapy. Cell 2015;160:977–89.
4. Letai AG. Diagnosing and exploiting cancer's addiction to blocks in apoptosis. Nat Rev Cancer 2008;8:121–32.
5. Tsujimoto Y, Yunis J, Onorato-Showe L, Erikson J, Nowell PC, Croce CM. Molecular cloning of the chromosomal breakpoint of B-cell lymphomas and leukemias with the t(11;14) chromosome translocation. Science 1984;224:1403–6.
6. Faber AC, Corcoran RB, Ebi H, Sequist LV, Waltman BA, Chung E, et al. BIM expression in treatment-naive cancers predicts responsiveness to kinase inhibitors. Cancer Discov 2011;1:352–65.
7. Cragg MS, Kuroda J, Puthalakath H, Huang DC, Strasser A. Gefitinib-induced killing of NSCLC cell lines expressing mutant EGFR requires BIM and can be enhanced by BH3 mimetics. PLoS Med 2007;4:1681–89.
8. Deng J, Shimamura T, Perera S, Carlson NE, Cai D, Shapiro GI, et al. Proapoptotic BH3-only BCL-2 family protein BIM connects death signaling from epidermal growth factor receptor inhibition to the mitochondrion. Cancer Res 2007;67:11867–75.
9. Gong Y, Somwar R, Politi K, Balak M, Chmielecki J, Jiang X, et al. Induction of BIM is essential for apoptosis triggered by EGFR kinase inhibitors in mutant EGFR-dependent lung adenocarcinomas. PLoS Med 2007;4:e294.
10. Costa DB, Halmos B, Kumar A, Schumer ST, Huberman MS, Boggon TJ, et al. BIM mediates EGFR tyrosine kinase inhibitor-induced apoptosis in lung cancers with oncogenic EGFR mutations. PLoS Med 2007;4:1669–79.
11. Delbridge AR, Grabow S, Strasser A, Vaux DL. Thirty years of BCL-2: translating cell death discoveries into novel cancer therapies. Nat Rev Cancer 2016;16:99–109.
12. Cory S, Roberts AW, Colman PM, Adams JM. Targeting BCL-2-like proteins to kill cancer cells. Trends Cancer 2016;2:443–60.
13. Hata AN, Engelman JA, Faber AC. The BCL2 family: key mediators of the apoptotic response to targeted anticancer therapeutics. Cancer Discov 2015;5:475–87.
14. Holohan C, Van Schaeybroeck S, Longley DB, Johnston PG. Cancer drug resistance: an evolving paradigm. Nat Rev Cancer 2013;13:714–26.
15. Ng KP, Hillmer AM, Chuah CT, Juan WC, Ko TK, Teo AS, et al. A common BIM deletion polymorphism mediates intrinsic resistance and inferior responses to tyrosine kinase inhibitors in cancer. Nat Med 2012;18:521–8.
16. Hata AN, Yeo A, Faber AC, Lifshits E, Chen Z, Cheng KA, et al. Failure to induce apoptosis via BCL-2 family proteins underlies lack of efficacy of combined MEK and PI3K inhibitors for KRAS-mutant lung cancers. Cancer Res 2014;74:3146–56.
17. Conrad M, Angeli JP, Vandenabeele P, Stockwell BR. Regulated necrosis: disease relevance and therapeutic opportunities. Nat Rev Drug Discov 2016;15:348–66.
18. Vanden Berghe T, Linkermann A, Jouan-Lanhouet S, Walczak H, Vandenabeele P. Regulated necrosis: the expanding network of non-apoptotic cell death pathways. Nat Rev Mol Cell Biol 2014;15:135–47.
19. Wallach D, Kang TB, Dillon CP, Green DR. Programmed necrosis in inflammation: Toward identification of the effector molecules. Science 2016;352:aaf2154.
20. Holler N, Zaru R, Micheau O, Thome M, Attinger A, Valitutti S, et al. Fas triggers an alternative, caspase-8-independent cell death pathway using the kinase RIP as effector molecule. Nat Immunol 2000;1:489–95.
21. Degterev A, Hitomi J, Germscheid M, Ch'en IL, Korkina O, Teng X, et al. Identification of RIP1 kinase as a specific cellular target of necrostatins. Nat Chem Biol 2008;4:313–21.
22. Zhang DW, Shao J, Lin J, Zhang N, Lu BJ, Lin SC, et al. RIP3, an energy metabolism regulator that switches TNF-induced cell death from apoptosis to necrosis. Science 2009;325:332–6.
23. Cho YS, Challa S, Moquin D, Genga R, Ray TD, Guildford M, et al. Phosphorylation-driven assembly of the RIP1-RIP3 complex regulates programmed necrosis and virus-induced inflammation. Cell 2009;137:1112–23.
24. He S, Wang L, Miao L, Wang T, Du F, Zhao L, et al. Receptor interacting protein kinase-3 determines cellular necrotic response to TNF-alpha. Cell 2009;137:1100–11.
25. Sun L, Wang H, Wang Z, He S, Chen S, Liao D, et al. Mixed lineage kinase domain-like protein mediates necrosis signaling downstream of RIP3 kinase. Cell 2012;148:213–27.

26. Zhao J, Jitkaew S, Cai Z, Choksi S, Li Q, Luo J, et al. Mixed lineage kinase domain-like is a key receptor interacting protein 3 downstream component of TNF-induced necrosis. Proc Natl Acad Sci U S A 2012;109:5322–7.
27. Cai Z, Jitkaew S, Zhao J, Chiang HC, Choksi S, Liu J, et al. Plasma membrane translocation of trimerized MLKL protein is required for TNF-induced necroptosis. Nat Cell Biol 2014;16:55–65.
28. Dondelinger Y, Declercq W, Montessuit S, Roelandt R, Goncalves A, Bruggeman I, et al. MLKL compromises plasma membrane integrity by binding to phosphatidylinositol phosphates. Cell Rep 2014;7:971–81.
29. Wang H, Sun L, Su L, Rizo J, Liu L, Wang LF, et al. Mixed lineage kinase domain-like protein MLKL causes necrotic membrane disruption upon phosphorylation by RIP3. Mol Cell 2014;54:133–46.
30. Hildebrand JM, Tanzer MC, Lucet IS, Young SN, Spall SK, Sharma P, et al. Activation of the pseudokinase MLKL unleashes the four-helix bundle domain to induce membrane localization and necroptotic cell death. Proc Natl Acad Sci U S A 2014;111:15072–7.
31. Chen X, Li W, Ren J, Huang D, He WT, Song Y, et al. Translocation of mixed lineage kinase domain-like protein to plasma membrane leads to necrotic cell death. Cell Res 2014;24:105–21.
32. Shi J, Zhao Y, Wang K, Shi X, Wang Y, Huang H, et al. Cleavage of GSDMD by inflammatory caspases determines pyroptotic cell death. Nature 2015;526:660–5.
33. Kayagaki N, Stowe IB, Lee BL, O'Rourke K, Anderson K, Warming S, et al. Caspase-11 cleaves gasdermin D for non-canonical inflammasome signalling. Nature 2015;526:666–71.
34. He WT, Wan H, Hu L, Chen P, Wang X, Huang Z, et al. Gasdermin D is an executor of pyroptosis and required for interleukin-1beta secretion. Cell Res 2015;25:1285–98.
35. Rogers C, Fernandes-Alnemri T, Mayes L, Alnemri D, Cingolani G, Alnemri ES. Cleavage of DFNA5 by caspase-3 during apoptosis mediates progression to secondary necrotic/pyroptotic cell death. Nat Commun 2017;8:14128.
36. Wang Y, Gao W, Shi X, Ding J, Liu W, He H, et al. Chemotherapy drugs induce pyroptosis through caspase-3 cleavage of a gasdermin. Nature 2017;547:99–103.
37. Zhang S, Zhang M, Jing Y, Yin X, Ma P, Zhang Z, et al. Deubiquitinase USP13 dictates MCL1 stability and sensitivity to BH3 mimetic inhibitors. Nat Commun 2018;9:215.
38. Gridelli C, Rossi A, Carbone DP, Guarize J, Karachaliou N, Mok T, et al. Non-small-cell lung cancer. Nat Rev Dis Primers 2015;1:15009.
39. Melnikov VY, Faubel S, Siegmund B, Lucia MS, Ljubanovic D, Edelstein CL. Neutrophil-independent mechanisms of caspase-1- and IL-18-mediated ischemic acute tubular necrosis in mice. J Clin Invest 2002;110:1083–91.
40. Dixon SJ, Lemberg KM, Lamprecht MR, Skouta R, Zaitsev EM, Gleason CE, et al. Ferroptosis: an iron-dependent form of nonapoptotic cell death. Cell 2012;149:1060–72.
41. Andrabi SA, Dawson TM, Dawson VL. Mitochondrial and nuclear cross talk in cell death: parthanatos. Ann N Y Acad Sci 2008;1147:233–41.
42. Syntichaki P, Xu K, Driscoll M, Tavernarakis N. Specific aspartyl and calpain proteases are required for neurodegeneration in C. elegans. Nature 2002;419:939–44.
43. Clarke SJ, McStay GP, Halestrap AP. Sanglifehrin A acts as a potent inhibitor of the mitochondrial permeability transition and reperfusion injury of the heart by binding to cyclophilin-D at a different site from cyclosporin A. J Biol Chem 2002;277:34793–9.
44. Kimura T, Takabatake Y, Takahashi A, Isaka Y. Chloroquine in cancer therapy: a double-edged sword of autophagy. Cancer Res 2013;73:3–7.
45. Chen X, He WT, Hu L, Li J, Fang Y, Wang X, et al. Pyroptosis is driven by non-selective gasdermin-D pore and its morphology is different from MLKL channel-mediated necroptosis. Cell Res 2016;26:1007–20.
46. Van Laer L, Huizing EH, Verstreken M, van Zuijlen D, Wauters JG, Bossuyt PJ, et al. Nonsyndromic hearing impairment is associated with a mutation in DFNA5. Nat Genet 1998;20:194–7.
47. Akino K, Toyota M, Suzuki H, Imai T, Maruyama R, Kusano M, et al. Identification of DFNA5 as a target of epigenetic inactivation in gastric cancer. Cancer Sci 2007;98:88–95.
48. Kim MS, Lebron C, Nagpal JK, Chae YK, Chang X, Huang Y, et al. Methylation of the DFNA5 increases risk of lymph node metastasis in human breast cancer. Biochem Biophys Res Commun 2008;370:38–43.
49. Yokomizo K, Harada Y, Kijima K, Shinmura K, Sakata M, Sakuraba K, et al. Methylation of the DFNA5 gene is frequently detected in colorectal cancer. Anticancer Res 2012;32:1319–22.
50. Sharma SV, Lee DY, Li B, Quinlan MP, Takahashi F, Maheswaran S, et al. A chromatin-mediated reversible drug-tolerant state in cancer cell subpopulations. Cell 2010;141:69–80.